Journal of Physics: Conference Series **767** (2016) 012004 doi:10.1088/1742-6596/767/1/012004

Charge-to-mass dependence of heavy ion spectral breaks in large gradual solar energetic particle events

M. I. Desai[1,2], G. M. Mason[3], M. A. Dayeh[1], R. W. Ebert[1], D. J. McComas[4], G. Li[5], C. M. S. Cohen[6], R. A. Mewaldt[6], N. A. Schwadron[7], and C. W. Smith[7]

[1]Southwest Research Institute, 6220 Culebra Road, San Antonio, TX 78023, USA
[2]University of Texas at San Antonio, One UTSA Circle, San Antonio, TX 78249, USA
[3]Johns Hopkins University/Applied Physics Laboratory, Laurel, MD 20723, USA
[4]Department of Astrophysical Sciences, Princeton University, NJ 08544, USA
[5]CSPAR, University of Alabama in Huntsville, Huntsville, AL 35756, USA
[6]California Institute of Technology, Pasadena, CA 91125, USA
[7]University of New Hampshire, 8 College Road, Durham, NH 03824, USA

E-mail: mdesai@swri.edu

Abstract. We fit the ∼0.1-500 MeV/nucleon H-Fe spectra in 46 large SEP events surveyed by [1] with the double power-law Band function to obtain a normalization constant, low- and high-energy parameters γ_a and γ_b; and break energy E_B. We also calculate the low-energy power-law spectral slope γ_1. We find that: 1) γ_a, γ_1, and γ_b are species-independent within a given SEP event, and the spectra steepen with increasing energy; 2) E_B's are well ordered by Q/M ratio, and decrease systematically with decreasing Q/M, scaling as $(Q/M)^{\alpha}$ with α varying between ∼0.2-3; 3) α is well correlated with Fe/O at ∼0.16-0.23 MeV/nucleon and CME speed; 4) In most events: α <1.4 and the spectra steepen significantly at higher energy with γ_b-γ_a >3; and 5) Seven out of nine extreme SEP events (associated with faster CMEs and GLEs) are Fe-rich and have α >1.4 with flat spectra at low and high energies yielding γ_b-γ_a <3. The species-independence of γ_a, γ_1, and γ_b and the systematic Q/M dependence of E_B within an event, as well as the range of values for α suggest that the formation of double power-laws in SEP events occurs primarily due to diffusive acceleration at near-Sun CME shocks and not due to scattering in the interplanetary turbulence. In most events, the Q/M-dependence of E_B is consistent with the equal diffusion coefficient condition while the event-to-event variations in α are probably driven by differences in the near-shock wave intensity spectra, which are flatter than the Kolmogorov turbulence spectrum but still weaker compared to that inferred for the extreme events. The weaker turbulence allows SEPs to escape more easily, resulting in weaker Q/M-dependence of E_B, (lower α values) and spectral steepening at higher energies. In extreme events, the flatter spectra at high- and low-energy and stronger Q/M-dependence of E_B (larger α values) occur due to enhanced wave power, which also enables the faster CME shocks to accelerate flare suprathermals more efficiently than ambient coronal ions.

1. Introduction

Large gradual solar energetic particle (SEP) events are believed to be accelerated via diffusive shock acceleration (DSA) mechanisms at shock waves driven by fast coronal mass ejections (CMEs) that plough through the solar corona and interplanetary (IP) medium (e.g., [2–4]). Such large SEP events, if sufficiently intense, can significantly increase radiation levels in the

near-Earth environment, thus damaging technological assets and adversely affecting the health and safety of humans in space (e.g., [5]). Previous studies have shown that the differential energy spectra of H-Fe nuclei in large SEP events exhibit two distinct (or broken) power-laws above and below a characteristic roll-over or break energy, with the break energy typically decreasing for the heavier ion species, or more precisely, with the ion's charge-to-mass or Q/M ratio (e.g., [6–9]). [10] suggested that this systematic Q/M-dependence occurs because the energy spectra, usually plotted in MeV/nucleon, steepen or roll over at the same value of the diffusion coefficient for different species, which depends on ion rigidity or the Q/M ratio (see [10–12]). [10] also showed that this behavior can be characterized by $\frac{E_X}{E_H} \propto (\frac{Q_X}{M_X})^{\alpha}$, where E_X is the spectral break energy of species X; E_H is the spectral break energy of H; and Q_X and M_X are the ionic charge and atomic mass of species X.

2. Instrumentation, Event Selection, and Data Analyses

We use energetic ion data from (1) the Ultra-Low-Energy Isotope Spectrometer (ULEIS: [13]); (2) the Solar Isotope Spectrometer (SIS: [14]); and the Electron, Proton, and Alpha monitor (EPAM: [15]) on board NASA's Advanced Composition Explorer (ACE: [16]) launched in 1997 August. We also use proton data from the Proton and Electron Telescope (PET) on board the Solar, Anomalous, and Magnetospheric Particle Explorer (SAMPEX/PET: [17]); the Energetic and Relativistic Nuclei and Electron experiment (ERNE: [18]) on board the joint ESA/NASA Solar and Heliospheric Observatory (SoHO); and the Energetic Particle Sensor (EPS) on NOAA's Geostationary Operational Environmental Satellites (GOES, series 8-15).

[1] describes our event selection criteria and method for identifying sampling intervals for 46 isolated, large SEP events observed at 1 AU from November 1997 through April 2014 that were not accompanied by ≥0.1 MeV/nucleon intensity enhancements associated with the passage of in-situ CME-driven IP shocks (e.g., [19]). Such enhancements are known as Energetic Storm Particles or ESPs. For each of these 46 SEP events, we followed the [20] procedure and used ULEIS and SIS oxygen time-intensity profiles and 1/ion speed spectrograms (see Figure 1) to select energy-dependent sampling intervals to account for velocity dispersion caused by the later arrival of slower ions compared to the faster ions. An example of the application of this technique is shown as the red trapezoid in Figure 1b. This interval also includes an IP shock that arrived at ACE at 2116 UT on 2011 November 28 (`http://www.srl.caltech.edu/ACE/ASC/DATA/Shocks/shocks_good.html`). This SEP event was included in our survey because the in-situ CME shock was not accompanied by a significant local ESP event above ∼0.1 MeV/nucleon.

Tables 1 and 2 of [1] provide the solar source properties, fluence sampling intervals, the ∼0.5-2.0 MeV/nucleon ^{3}He/^{4}He ratio, and the Fe/O ratios at ∼0.16-0.23 MeV/nucleon and ∼15-21 MeV/nucleon associated with these 46 events. In this study for each SEP event, we used ACE/ULEIS, ACE/SIS, GOES/EPS, SoHO/ERNE, and when available, SAMPEX/PET, to obtain the event-integrated ∼0.1-500 MeV/nucleon fluence spectra for 11 species in the range H-Fe, as shown in the three examples in Figure 2. The proton spectra from various instruments in each SEP event at overlapping energies are in excellent agreement within the stated ∼20% uncertainties that account for differences between various instruments (see [21]).

We fit each spectrum using the non-linear least-squares Levenberg-Marquardt technique and minimized the χ^2 to fit the 4 parameter Band function (see [22]; Eq. 1) given by:

$$\begin{aligned} dJ/dE &= CE^{-\gamma_a} \exp\left(-\tfrac{E}{E_B}\right) \textbf{ for } E \le (\gamma_b - \gamma_a)\, E_B \\ dJ/dE &= CE^{-\gamma_b} \left[(\gamma_b - \gamma_a)\, E_B\right]^{\gamma_b - \gamma_a} \exp\left(\gamma_b - \gamma_a\right) \textbf{ for } E \ge (\gamma_b - \gamma_a)\, E_B \end{aligned} \quad (1)$$

Here C is the normalization constant, γ_a and γ_b are the low-energy and high-energy Band-parameters, and E and E_B are the kinetic and spectral break energy, respectively. Units of E

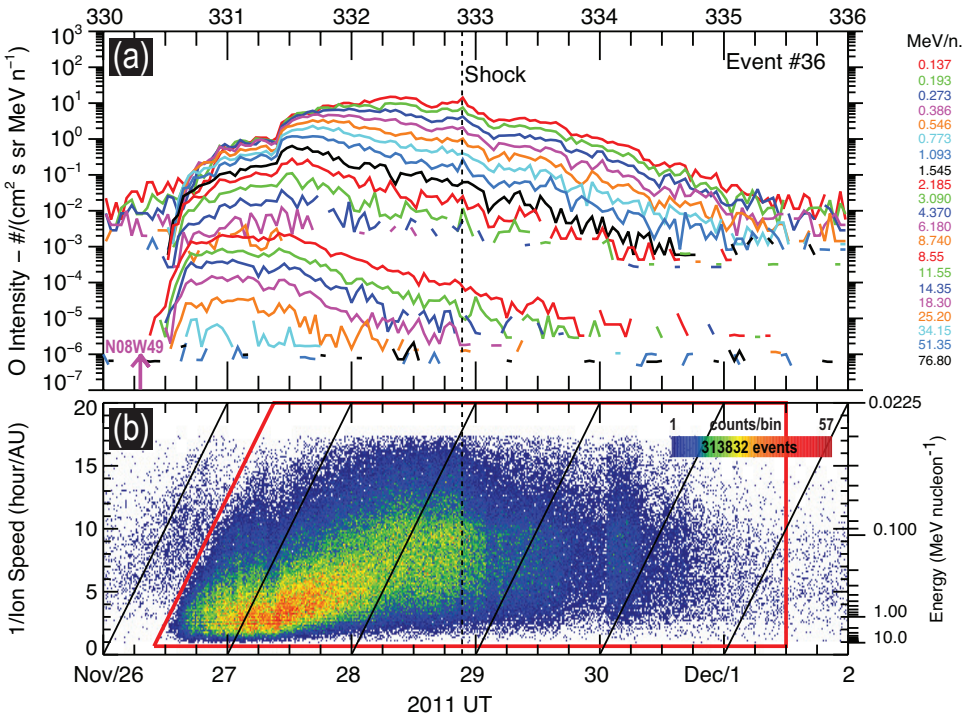

Figure 1. (a) Hourly-averaged time-intensity profiles of ∼0.1-100 MeV/nucleon oxygen nuclei measured by ACE/ULEIS and ACE/SIS during a large gradual solar energetic particle (SEP) event that occurred on 2011 November 26-December 1. The pink arrow indicates the flare occurrence time. (b) 1/ion speed spectrogram of ∼0.1-10 MeV/nucleon C-Fe nuclei measured by ULEIS. The red region represents the SEP sampling interval that accounts for velocity dispersion of ions traveling along a 1.2 AU path length (slanted black lines). The arrival time of an IP shock at ACE on 2011 November 28, 2116 UT is taken from the ACE IP shock list; see [1] for more details.

and E_B are MeV/nucleon. For each Band-fit parameter, we obtain the formal 1σ uncertainty from the off-diagonal terms of the covariance matrix [23]. As discussed in [1], we found that for most species in most SEP events (see Figures 2a, 2c, and 2e), the fits are visually and statistically reasonable, with reduced χ^2 values having ∼50% probabilities (also see [9]). Note that the Band function has no physical basis, and we use it here because it helps us to characterize the behavior of SEP spectra over a broad energy range using only 4 free parameters.

Table 2 in [21] provides the H, O, and Fe Band function fit parameters for the 46 SEP events. For each SEP event, we also fitted the roll-over or break energy E_X of each species X normalized to the proton spectral break energy, E_H with a linear function of the form $\log(\frac{E_X}{E_H}) = \log(n_0) + \alpha\ \log(\frac{Q_X}{M_X})$, whose slope α is the power-law exponent discussed in Section 1. Examples of three different types of Q/M-dependence of E_X/E_H, i.e., three different values for α, are shown in Figures 2b, 2d, and 2f.

3. Properties of Spectral Slopes

[1] shows that the non-orthognality of the Band function results in strong coupling between the O Band-parameters γ_a and E_B, and that γ_a can be significantly different from what is commonly described as the low-energy power-law spectral slope γ_1. In order to obtain a physically meaningful quantity that represents the low-energy portion of the SEP spectra below the break energies more accurately, we calculate the low-energy spectral slope γ_1 between ∼0.1-

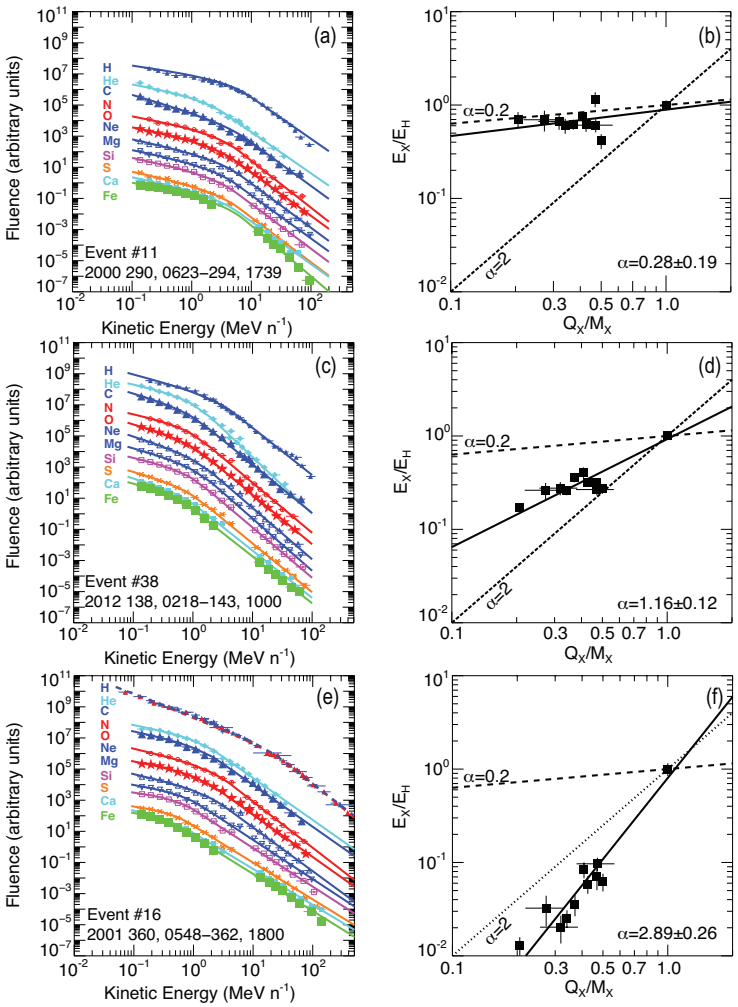

Figure 2. (a, c, e) Event-integrated differential fluences versus energy of ∼0.1-500 MeV/nucleon H-Fe nuclei during 3 large SEP events. The energy spectra for different species are offset for clarity. Solid lines are fits to the spectra using the Band function (see Eq. 1; [22]). In all panels, the H spectra (top-most blue symbols) are from ACE/ULEIS, SoHO/ERNE, and GOES-8/EPS, and the He-Fe spectra are from ACE/ULEIS and ACE/SIS. In (e) red data points superposed on the top-most blue symbols are proton data from ACE/EPAM, GOES-8/EPS, and SAMPEX/PET, and the top-most dotted red-curve shows the corresponding Band-function fit from [9]. (b, d, f) Spectral break energy E_X of species X normalized to E_H – break energy of H vs. the ion's charge-to-mass (Q/M) ratio. The solid line is the fit to the data $\log(\frac{E_X}{E_H}) = \log(n_0) + \alpha \log(\frac{Q_X}{M_X})$. Dashed lines are the same equation with $\alpha = 2$, and dotted lines are the same equation with $\alpha = 0.2$.

1 MeV/nucleon for each species in all SEP events using Eq. 1 (top) and the corresponding Band-parameters γ_a and E_B.

Figure 3a shows a scatter plot of γ_b vs. γ_a obtained for each individual species in all SEP events. As seen for the O spectral slopes in [1], we note that most SEP spectra are flatter at lower energies and steepen above the break energy. Figures 3b and 3c investigate species-associated variations in (a) γ_1 and γ_a, and (b) γ_b within an event by plotting the distributions of their corresponding mean deviations. The mean deviation for each parameter in each event is calculated with respect to the corresponding species-averaged value of that parameter within that event. We note the following: (1) The mean deviations of γ_1, γ_a, and γ_b have narrow distributions that result in well-behaved Gaussian-like distributions (black curves) with small 1σ values. These results indicate that, within a given SEP event, the three parameters γ_1, γ_a, and γ_b, have remarkably similar values for all species, for each event, both the low-energy and high-energy spectral slopes are similar within ∼10-15%. Thus, in a given event, species-associated spectral variations are driven primarily by differences in the break energy at which the spectra steepen. Three examples of such species-associated differences in E_B are shown in Figures 2b, 2d, and 2f (see [21]).

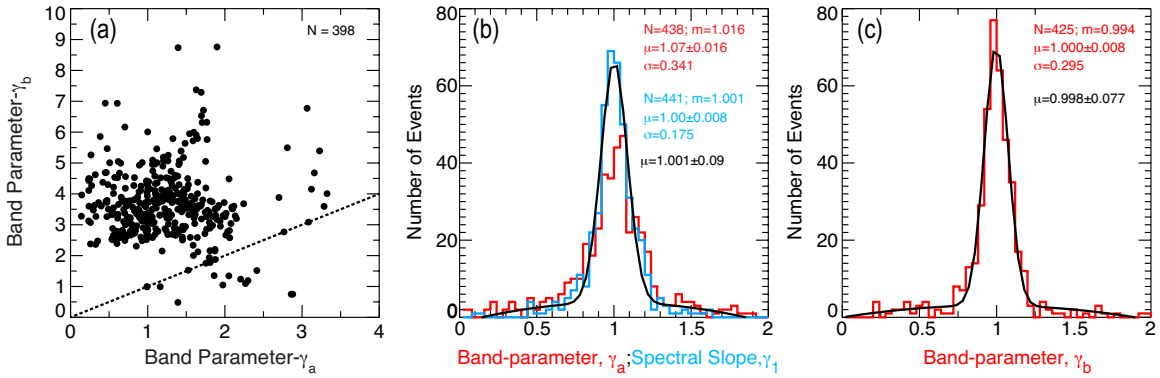

Figure 3. (a) Scatter-plots of γ_a vs. γ_b. Dotted line shows spectra for which $\gamma_a = \gamma_b$. All parameters with relative uncertainties >100% are excluded. Histograms of mean deviations of the (b) Band-parameter γ_a (red), and low-energy spectral slope γ_1 (blue); and (c) Band-parameter, γ_b from the corresponding species-averaged value in each event. N=number of data points; m=median; μ=mean and standard error of the mean; and σ=1 standard deviation of the distribution. The solid black curves show Gaussian fits, with mean and 1σ standard deviation, for the distributions of γ_1 in (a) and γ_b.

4. Properties of Power-Law Exponent α

Figure 4 investigates (a) the statistical properties of α and its relationship with (b) CME speed, (c) the ∼0.16-0.23 MeV/nucleon Fe/O ratio, and (d) the difference between the high- and low-energy Band parameters $\gamma_b - \gamma_a$. Figure 4a shows the histogram of α along with the mean, standard deviation, and median value of the distribution. The CME speeds are obtained from `http://umbra.nascom.nasa.gov/SEP/`, `ftp://ftp.ngdc.noaa.gov/STP/swpc_products/daily_reports/solar_event_reports/`, `cdaw.gsfc.nasa.gov/CME_list/` ([24–27]). For the 33 events shown in Figure 4 we note the following.

(i) α has a mean value of 1.27, median value of 1.16, and lies between ∼0.2-3, with values for 3 SEP events greater than 2; two of these events were also accompanied by Ground Level Enhancements or GLEs (e.g., see Figure 1f).

(ii) α exhibits statistically significant, positive trends with the CME speed and Fe/O ratio, with values for correlation coefficients of r ∼0.414 and r ∼0.39, respectively, which have probabilities of <2.5% of being exceeded by uncorrelated pairs of parameters. It is also evident that the correlations with both the CME speed and Fe/O are largely due to the presence of events associated with high CME speeds and GLEs.

(iii) α is not correlated with $\gamma_b - \gamma_a$, but SEP events with α ∼0.2-1.4 exhibit a larger range of values for $\gamma_b - \gamma_a$, i.e., events for which the spectra steepen significantly at higher energies have α values between ∼0.6-1.4. Figure 4d also shows that extreme SEP events have $\alpha \geq 1.4$ and $\gamma_b - \gamma_a < 3.$, i.e., extreme SEP events have stronger Q/M-dependence in E_B's and flatter spectra at high and low energies.

5. Summary and Discussion

We fit the event-integrated fluence spectra of ∼0.1-500 MeV/nucleon H-Fe in the 46 SEP events with the 4 parameter Band function and investigate properties of the SEP Band-parameters γ_a, γ_b, and E_B (also see [21]). We also calculate the low-energy power-law spectral slope γ_1. Our results are:

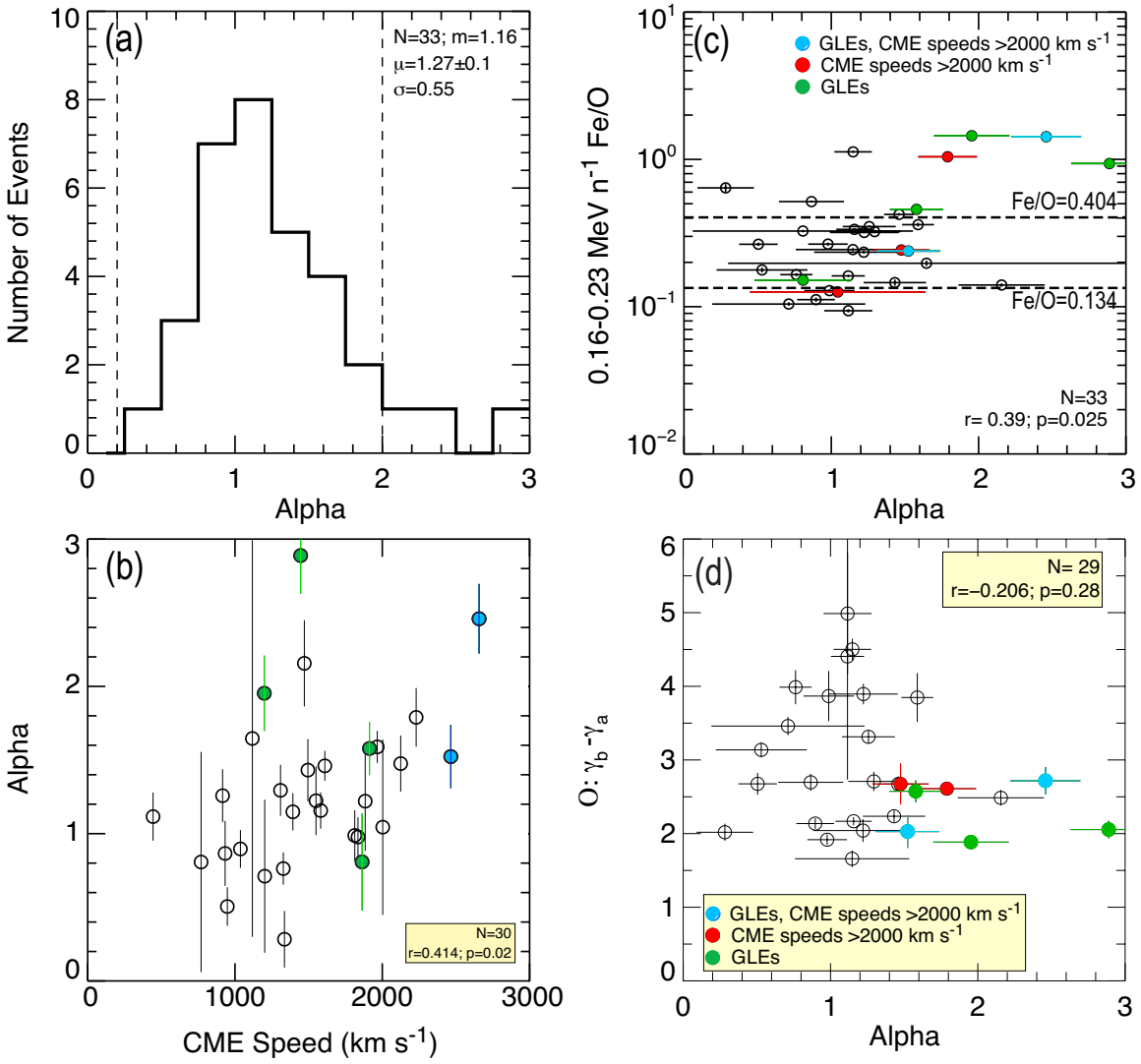

Figure 4. (a) Histogram of α. (b) α vs. CME speed (km/s). (c) α vs. ~0.16-0.23 MeV/nucleon Fe/O. (d) α vs. the difference $\gamma_b - \gamma_a$. N=number of events plotted; μ, σ, and m as defined in Figure 3; r=correlation coefficient and p=probability that the absolute value of r can be exceeded by an uncorrelated pair of parameters. Green symbols show SEP events accompanied by Ground Level Enhancements or GLEs, red symbols denote SEP events associated with CMEs that have speeds >2000 km/s, blue symbols are SEPs that were accompanied by GLEs and >2000 km/s speed CMEs. Dashed lines show Fe/O ratios at 0.404 and 0.134, which are average values in several large SEP events at ~0.32-0.5 MeV/nucleon [20] and at ~5-12 MeV/nucleon [28], respectively.

(i) Figures 2b, 2d, and 2f show that the E_B's in 3 SEP events vary systematically according to the ion's Q/M ratio. We also find that this dependence can be characterized by a single parameter α – given by fitting a linear function of the form $\log(\frac{E_X}{E_H}) = \log(n_0) + \alpha \log(\frac{Q_X}{M_X})$ – in 33 of the 46 events surveyed.

(ii) Figure 3a shows that γ_a lies between ~0.1-3 and γ_b lies between ~0.5-9. γ_a is also typically smaller than γ_b, implying that the energy spectrum of each species in a given event steepens with increasing energy.

(iii) Figures 3b and 3c show that in a given SEP event, γ_a, γ_1, and γ_b are species-independent, since the mean deviation of each parameter exhibits a Gaussian-like distribution with a small 1σ of $\leq$0.08.

(iv) Figure 4a shows that for 33 SEP events, α varies between $\sim$0.2-3. SEPs associated with GLEs and faster CMEs with speeds >2000 km/s have $\alpha \geq 1.4$ vs. $\alpha < 1.4$ for the rest of the events.

(v) Figures 4b and 4c show that α exhibits statistically significant positive trends with both, the CME speed and the $\sim$0.16-0.23 MeV/nucleon Fe/O; extreme SEPs are associated with the fastest CMEs and highest Fe/O ratios.

(vi) Figure 4d shows that α is not correlated with the difference in the spectral slopes $\gamma_b - \gamma_a$; $\gamma_b - \gamma_a$ varies between $\sim$2-5 in events with $\alpha \leq 1.4$, while extreme SEPs have $\alpha \geq 1.4$ and $\gamma_b - \gamma_a < 3$.

5.1. Properties of CME shocks and associated turbulence

Comparing our survey to prior studies, we note that some of the 5 events studied by [10] and [12] also included the local shock-accelerated ESP component that accompanied the larger SEP event. In contrast, we eliminate all events with possible contributions from local IP shock-associated populations (see [1]). Further, we use event-integrated fluences, rather than time-intensity profiles (see [29]), to study the SEP spectral properties. In particular, [29] used a detailed model of IP propagation and showed that transport from the inner solar system can lower the break energy systematically for all species, as well as lower the slopes by $\sim$10-20%, but that the basic spectral form remains intact (see Fig. 14 in [29]). Alternatively, we note that [30] fitted the double power-law proton spectra in 9 of the 16 GLE events studied by [10] with an analytical model that included interplanetary transport effects, and found that single power-law spectra injected by CME shocks near the Sun can exhibit spectral breaks at 1 AU due to scatter-dominated transport through the interplanetary medium. However, the [30] model predicts that α in GLE-associated SEP events should lie in the range $\sim$0.18-0.75, which is clearly inconsistent with the $\alpha > 1.58$ observed in 5 of the 7 GLEs in our survey (see Figures 2f and 4). On this basis, we contend that the formation of the double power-law SEP spectra, their associated properties, and the observed Q/M-dependence of E_B primarily reflect conditions near the distant CME-driven shocks where the acceleration takes place, and are not significantly affected by contributions from local interplanetary shock-accelerated populations nor by Q/M-dependent transport and scattering in the interplanetary turbulence en route to 1 AU (e.g., see [12; 29; 31]).

A fundamental prediction of early 1-dimensional (1D) steady-state (as well as the more recent time-dependent DSA-based SEP models) is that, in a given event, the differential energy spectrum of the accelerated particles below the break energy is characterized by a low-energy power-law spectral slope γ given by $\frac{dj}{dE} \propto E^{-\gamma}$ (e.g., [4; 32–34]). These models also predict that γ is independent of ion species, and is determined solely by $\gamma \approx (H+2)/(2H-2)$, where H is the strength or compression ratio of the CME-driven shock. Our results show that both, the SEP Band-parameter γ_a and the low-energy spectral slope γ_1 in a given SEP event are remarkably similar for all species, and that such species-independent spectral slopes are observed at both low and high energies for most of the events in our survey. We therefore suggest that, to first order, the formation of double power-law spectra in large SEP events is consistent with DSA at near-Sun CME shocks (e.g., [34]).

We now use the DSA-predicted relationship between γ (here we use the species-averaged γ_1 for each event) and H to infer compression ratios of near-Sun CME shocks. Figure 5a compares the relationship between the inferred compression ratio and CME speed. The figure shows that the inferred shock compression ratios in 37 events lie between $\sim$1-5.5, with $H > 4$ for 4 events.

These values are consistent with the predicted range of values for CME shock compression ratios in large SEP events (see [34]), and are also well within the constraints of the Rankine-Hugoniot discontinuity conditions for the allowable range of ∼1-4 and upper limit of < 4 for shocks in non-relativistic plasmas (e.g., [35]). We note that all cases of $H > 4$ have sizeable uncertainties. H also exhibits a weak but positive correlation with CME speed; for 37 events, a value of r ∼0.38 has <2% probability, and excluding the 4 events with $H > 4$, yields r ∼0.32 which has <7% chance of being exceeded by uncorrelated pairs of parameters.

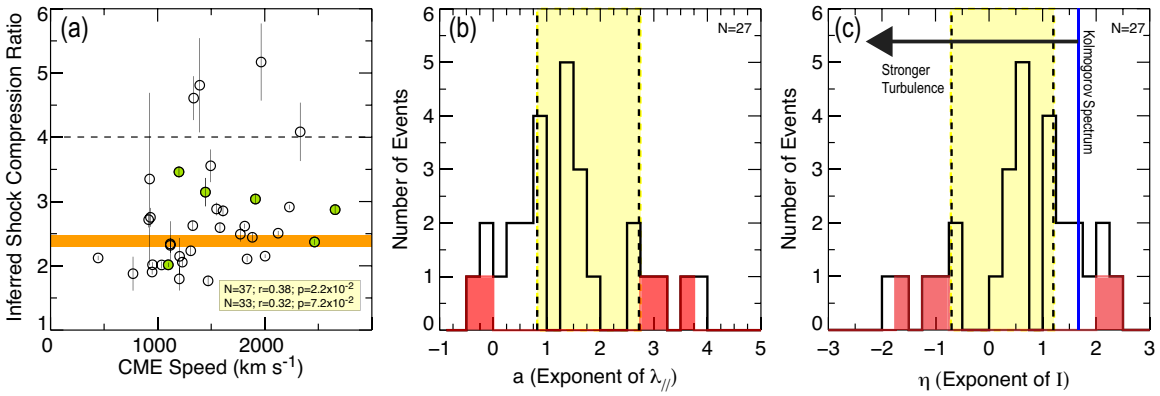

Figure 5. (a) Scatterplot of the inferred shock compression ratio vs. CME speed. Histograms of (b) a, the inferred power-law exponent of the M/Q-dependence of the scattering mean free path $\lambda_{\parallel} \propto (M/Q)^a$, and (c) η, the inferred power-law exponent of the wave intensity spectrum I near the CME-driven shock given by $I \propto k^{-\eta}$. Green data points in (a) denote GLEs. Orange shaded region in (a) encompasses the mean value and the standard error of the mean, calculated by excluding the 4 outliers with values >4 and the six GLE events. Shaded yellow regions in (b) and (c) depict the range of values inferred by [12] for 5 large SEP events. Blue vertical line in (c) represents $\eta = 5/3$ – the typical interplanetary Kolmogorov spectrum; red histograms represent 5 GLE events.

The heavy ion fluence spectra in most SEP events are flat at energies below ∼1 MeV/nucleon and steepen above a roll-over or break energy, which decreases systematically with the ion's Q/M ratio. The Q/M-dependence of E_B's in a given SEP event is well represented by the function $\log(\frac{E_X}{E_H}) = \log(n_0) + \alpha \ \log(\frac{Q_X}{M_X})$ and characterized by the power-law exponent α. The values of α in 33 SEP events lie between ∼0.2-3, which encompasses the range of α values found by [10; 12]. Thus, with the exception of 3 events with $\alpha > 2$ (see Figure 4a), the range of values for α in our survey is consistent with the corresponding range of ∼0.2-2 predicted by [36]. In this model, the Q/M-dependence of the spectral break energies in a given SEP event occurs due to the "equal diffusion coefficient" or the "equal acceleration time" condition, and the event-to-event variations in the power-law exponent α are driven by the differences in the slopes of the turbulence spectra expected near shocks with different obliquity.

Assuming that the spectral break energies for different species in a given SEP event occur at the same value of the diffusion coefficient $\kappa_{\parallel}$, which scales as $(M/Q)^a$ with observed values of $a \approx 0.8 - 2.7$, [12] followed [37] and inferred that the power-law index η of the turbulence or wave intensity spectrum, given by $I(k) \propto k^{-\eta}$, near the CME shock acceleration region, ranged between 1.2 to -0.7. Here $\eta = 2 - a$, and a is related to the exponent α in our survey by $a = \alpha(2 - \alpha)$. We now follow the approach of [10; 12] to infer the power-law exponent a, which determines the scaling between the particle diffusion coefficient and the ion's M/Q ratio, and the power-law index η of the wave intensity spectrum for 27 SEP events in our survey. In this analysis, we only include events that satisfied the following: 1) fitted values of α and the

inferred values of a and η have relative uncertainties <100%, and 2) $-4 < \eta < +4$.

Figure 5 plots histograms of (b) a and (c) η, calculated using the values of α in 27 SEP events. Note that within the estimated uncertainties, a in 15 out of 27 SEP events lies in the range ∼0.75-2.75 and is comparable to that obtained by [12], as shown by the yellow shaded region. Also, a varies between ∼-0.33-3.9, which is roughly consistent with the typical range of ∼0.5-7 proposed recently by [34]; in this model $a < 1$ implies weak dependence of $\lambda_{\|}$ on the ion's Q/M ratio, while $a > 1$ indicates that $\lambda_{\|}$ depends strongly on Q/M (also see [36; 38–40]).

We remark that η in 27 events lies between -1.87 and 2.33; η in 15 events lies between ∼-0.7–1.2, as reported by [12]. In 9 events, $\eta > 1.2$ — the largest value reported by [12]. Overall, in 4 events $\eta > 5/3$, which represents cases where the turbulence intensity spectra near the distant CME shocks may be significantly steeper than the typical interplanetary Kolmogorov $k^{-5/3}$ turbulence spectrum. In contrast, $\eta \leq 5/3$ in 23 events, which implies that the turbulence spectra near the corresponding CME shocks are probably significantly flatter than the Kolmogorov spectrum.

5.2. Extreme SEP events and their implications for theoretical models

All 9 extreme SEP events have $\alpha \geq 1.4$, low values for γ_a, γ_b, and $\gamma_b - \gamma_a < 3$. This indicates that the corresponding spectra are relatively flat with similar spectral slopes at low and high energies. The fact that $\alpha > 2$ in 2 of the 7 GLE-associated SEP events in our study, taken together with the general result that higher values of $\alpha \geq 1.4$ are typically observed in SEP events that are also associated with faster CMEs and GLEs, indicates that spectral properties in these extreme SEP events are most likely governed by highly efficient trapping and stronger Q/M-dependent scattering due to substantially enhanced wave power near the distant CME-driven shocks (see also [12; 36]).

The above scenario is also consistent with the following inferred results shown in Figure 5:

(i) Figure 5a shows that the inferred values for the shock compression ratio H in extreme events tend to be somewhat larger than the event average, and that the correlations between H and α are likely to be driven by these events.

(ii) Figure 5b (red histograms) shows that $\lambda_{\|}$ has a strong Q/M-dependence with $a \geq 2.8$ in 3 events and $a < 0.2$ in 2 events.

(iii) Figure 5c (red histograms) shows that $\eta > 2$ or $\eta < -1.1$ in these 5 events, which corresponds to substantially enhanced wave power.

(iv) The 4 remaining extreme SEP events (not shown in Figures 5b and 5c) had amongst the strongest observed Q/M-dependence in E_B's, i.e., $\alpha > 1.6$, which results in $|\eta| > 4$.

The above results also imply that the scattering and trapping of particles near the distant CME shocks during at least 2 of the extreme SEP events is so strong that the Q/M-dependence of the spectral break energies exceeds the limit of the equal diffusion or equal resonance condition described by [36], thus indicating that the underlying mechanisms have not yet been fully incorporated in current theoretical models.

[41] reported that observations at several interplanetary shocks near 1 AU were consistent with their nonlinear guiding center theory-based model that described DSA at parallel and perpendicular shocks in the presence of wave excitation and ambient upstream turbulence, respectively. In this model, ambient turbulence near perpendicular shocks allows lower-energy particles to be accelerated as efficiently as parallel shocks, producing single power-law like spectra. In contrast, the equal resonance condition and occasional wave excitation near parallel shocks results in more efficient trapping and rapid acceleration of particles to higher energies, creating spectra that exhibit double power-laws or exponential roll-overs with the maximum energy scaling as $(Q/M)^{\alpha}$.

While our results are qualitatively consistent with the [41] model and other models in which the strongest Q/M dependence of the heavy ion spectral breaks occur at quasi-parallel shocks (e.g., [36]), we note that such shocks also have lower injection thresholds, and are therefore expected to primarily inject and accelerate the low-energy solar wind or ambient coronal ions (e.g., [42]; however, see [43] for an alternative viewpoint). In contrast, and consistent with the results reported in [1], we find that many of the extreme events that exhibit strong Q/M-dependent spectral break energies are also Fe-rich and ^{3}He-rich (see [21]). Specifically, we note that the ∼0.16-23 MeV/nucleon Fe/O ratio is enhanced between factors of ∼2-10 compared to the average SEP value of ∼0.134 in 7 of the 9 extreme SEP events, while the ∼0.5-2.0 MeV/nucleon ^{3}He/^{4}He ratio is enhanced by more than an order of magnitude over the corresponding solar wind value in 5 extreme SEPs (see [21]). This points to the importance of contributions of suprathermal flare-origin material to the seed populations for fast CME shocks, even in those cases where the turbulence levels are significantly enhanced and the shocks may be quasi-parallel. We suggest that in such events, the enhanced turbulence traps, injects, and accelerates the higher-energy suprathermals much more efficiently than the co-existing lower-energy solar wind or coronal suprathermal ions. Simultaneously, the equal diffusion coefficient condition causes the spectral break energies to exhibit stronger Q/M-dependence, occasionally exceeding the equal resonance condition limit, as in the case of 2 SEP events that produced GLEs. We suggest that our results can be reconciled with SEP models provided that they include suprathermal flare-origin material as an important component of the seed population that is available for acceleration at near-Sun CME shocks.

Acknowledgments
We are grateful to the members of the Space Physics Group at the University of Maryland and the Johns Hopkins Applied Physics Laboratory (JHU/APL) for the construction of the ULEIS instrument and to members of the Space Radiation Laboratory at the California Institute of Technology for the construction of the SIS instrument. We acknowledge use of the NOAA GOES and SoHO/ERNE proton data. Work at SwRI is partially supported by NASA grants NNX13AE07G and NNX13AI75G, NASA contracts NNX10AT75G and NNN06AA01C, and NSF Grants AGS-1135432 and AGS-1460118. Work at APL was supported by NASA grants NNX13AR20G/115828 and 44A- 1091698.

References

[1] Desai M I, Mason G M, Dayeh M A, Ebert R W, McComas D J, Li G, Cohen C M S, Mewaldt R A, Schwadron N A and Smith C W 2016 *The Astrophysical Journal* **816** 68

[2] Reames D V 1999 *Space Sci. Rev.* **90** 413–491

[3] Reames D V 2013 *Space Science Reviews,* 6

[4] Lee M A 2005 *Astrophys. J. Supplement Series* **158** 38–67

[5] Desai M I and Giacalone J 2016 *Living Reviews in Solar Physics* **5** 1

[6] McGuire R E, von Rosenvinge T T and McDonald F B 1984 *Solar/Interplanetary Intervals* ed Shea M A, Smart D F and McKenna-Lawlor S M P p 157

[7] Ellison D C and Ramaty R 1985 *Astrophys. J.* **298** 400–408

[8] Mazur J E, Mason G M, Klecker B and McGuire R E 1992 *Astrophysical Journal* **401** 398–410

[9] Mewaldt R A, Looper M D, Cohen C M S, Haggerty D K, Labrador A W, Leske R A, Mason G M, Mazur J E and von Rosenvinge T T 2012 *Space Sci. Rev.* **171** 97–120

[10] Mewaldt R A, Cohen C M S, Mason G M, Labradora A W, Looper M L, Haggerty D E, Maclennan C G, Cummings A C, Desai M I, Leske R A, Li G, Mazur J E, Stone E C and

Wiedenbeck M E 2005 *The Physics of Collisionless Shocks: 4th Annual IGPP. International Astrophysics Conference* (*ASP Conference Series* vol 781) ed Li G, Zank G P and Russell C T pp 227–232

[11] Tylka A J, Boberg P R, McGuire R E, Ng C K and Reames D V 2000 *Acceleration and Transport of Energetic Particles Observed in the Heliosphere* (*ASP Conference Series* vol 528) ed Mewaldt R A, Jokipii J R, Lee M A, Möbius E and Zurbuchen T H pp 147–152

[12] Cohen C M S, Stone E C, Mewaldt R A, Leske R A, Cummings A C, Mason G M, Desai M I, von Rosenvinge T T and Wiedenbeck M E 2005 *J. Geophys. Res.* **110** A09S16

[13] Mason G M, Gold R E, Krimigis S M, Mazur J E, Andrews G B, Daley K A, Dwyer J R, Heuerman K F, James T L, Kennedy M J, Lefevere T, Malcolm H, Tossman B and Walpole P H 1998 *Space Sci. Rev.* **86** 409–448

[14] Stone E C, Cohen C M S, Cook W R, Cummings A C, Gauld B, Kecman B, Leske R A, Mewaldt R A, Thayer M R, Dougherty B L, Grumm R L, Milliken B D, Radocinski R G, Wiedenbeck M E, Christian E R, Shuman S and von Rosenvinge T T 1998 *Space Science Reviews* **86** 357–408

[15] Gold R E, Krimigis S M, Hawkins S E I, Haggerty D K, Lohr D A, Fiore E, Armstrong T P, Holland G and Lanzerotti L J 1998 *Space Science Reviews* **86** 541–562

[16] Stone E C, Frandsen A M, Mewaldt R A, Christian E R, Margolies D, Ormes J F and Snow F 1998 *Space Science Reviews* **86** 1–22

[17] Cook W R, Cummings A C, Cummings J R, Garrard T L, Kecman B, Mewaldt R A, Selesnick R S, Stone E C, Baker D N and von Rosenvinge T T 1993 *IEEE Transactions on Geoscience and Remote Sensing (ISSN 0196-2892)* **31** 565–571

[18] Torsti J, Valtonen E, Lumme M, Peltonen P, Eronen T, Louhola M, Riihonen E, Schultz G, Teittinen M, Ahola K, Holmlund C, Kelha V, Leppälä K, Ruuska P and Strömmer E 1995 *Solar Physics* **162** 505–531

[19] Desai M I, Mason G M, Dwyer J R, Mazur J E, Gold R E, Krimigis S M, Smith C W and Skoug R M 2003 *The Astrophysical Journal* **588** 1149–1162

[20] Desai M I, Mason G M, Gold R E, Krimigis S M, Cohen C M S, Mewaldt R A, Mazur J E and Dwyer J R 2006 *Astrophys. J.* **649** 470–489

[21] Desai M I, Mason G M, Dayeh M A, Ebert R W, McComas D J, Li G, Cohen C M S, Mewaldt R A, Schwadron N A and Smith C W 2016 *submitted to The Astrophysical Journal*

[22] Band D, Matteson J, Ford L, Schaefer B, Palmer D, Teegarden B, Cline T, Briggs M, Paciesas W, Pendleton G, Fishman G, Kouveliotou C, Meegan C, Wilson R and Lestrade P 1993 *Astrophys. J.* **413** 281–292

[23] Markwardt C B 2009 *Astronomical Data Analysis Software and Systems XVIII ASP Conference Series* **411** 251

[24] Cane H V, Richardson I G and von Rosenvinge T T 2010 *Journal of Geophysical Research* **115** A08101

[25] Kahler S W 2013 *The Astrophysical Journal* **769** 110

[26] Ding L, Jiang Y, Zhao L and Li G 2013 *The Astrophysical Journal* **763** 30

[27] Richardson I G, von Rosenvinge T T, Cane H V, Christian E R, Cohen C M S, Labrador A W, Leske R A, Mewaldt R A, Wiedenbeck M E and Stone E C 2014 *Solar Physics* **289** 3059–3107

[28] Reames D V 2013 *Solar Physics* **astro-ph.SR(3)** 201–993

[29] Mason G M, Li G, Cohen C M S, Desai M I, Haggerty D K, Leske R A, Mewaldt R A and Zank G P 2012 *The Astrophysical Journal* **761** 104

[30] Li G and Lee M A 2015 *The Astrophysical Journal* **810** 82

[31] Zank G P, Rice W K M and Wu C C 2000 *J. Geophys. Res.* **105** 25079–25096

[32] Drury L O 1983 *Rep. Prog. Phys.* **46** 973–1027

[33] Schwadron N A, Lee M A, Gorby M, Lugaz N, Spence H E, Desai M I, Török T, Downs C, Linker J, Lionello R, Mikić Z, Riley P, Giacalone J, Jokipii J R, Kota J and Kozarev K 2015 *The Astrophysical Journal* **810** 97

[34] Schwadron N A, Lee M A, Gorby M, Lugaz N, Spence H E, Desai M I, Török T, Downs C, Linker J, Lionello R, Mikić Z, Riley P, Giacalone J, Jokipii J R, Kota J and Kozarev K 2015 *Journal of Physics: Conference Series* **642** 012025

[35] Viñas A F and Scudder J D 1986 *Journal of Geophysical Research (ISSN 0148-0227)* **91** 39

[36] Li G, Zank G P, Verkhoglyadova O, Mewaldt R A, Cohen C M S, Mason G M and Desai M I 2009 *Astrophys. J.* **702** 998–1004

[37] Dröge W 1994 *Astrophys. J. Suppl. Ser.* **90** 567–576

[38] Battarbee M, Laitinen T and Vainio R 2011 *Astronomy and Astrophysics* **535** A34

[39] Battarbee M, Vainio R, Laitinen T and Hietala H 2013 *Astronomy and Astrophysics* **558** A110

[40] Vainio R, Pönni A, Battarbee M, Koskinen H E J, Afanasiev A and Laitinen T 2014 *Journal of Space Weather and Space Climate* **4** A08

[41] Zank G P, Li G, Florinski V, Hu Q, Lario D and Smith C W 2006 *Journal of Geophysical Research* **111** A06108–16

[42] Tylka A J and Lee M A 2006 *Astrophys. J.* **646** 1319–1334

[43] Giacalone J 2005 *Astrophys. J.* **628** L37–L40